

ASCA observations of the iron K complex of Circinus X-1 near zero phase: spectral evidence for partial covering

W.N. Brandt,¹ A.C. Fabian,¹ T. Dotani,² F. Nagase,² H. Inoue,² T. Kotani³ and Y. Segawa²

¹ *Institute of Astronomy, Madingley Road, Cambridge CB3 0HA*

² *Institute of Space and Astronautical Science, Yoshino-dai, Sagamihara, Kanagawa 229, Japan*

³ *The Institute of Physical and Chemical Research (RIKEN), Hirosawa, 2-1, Wako-shi, Saitama 351-01, Japan*

1 February 2008

ABSTRACT

We report on *ASCA* energy spectra of Cir X-1 taken near its zero phase on 1994 August 4–5. The *ASCA* SIS detectors allow a much more detailed study of the iron K complex than has been possible before. We find that prior to a sudden upward flux transition the dominant iron K feature appears to consist of a large edge from neutral or nearly-neutral iron. The depth of the edge corresponds to an absorption column of $\approx 1.5 \times 10^{24} \text{ cm}^{-2}$, while little absorption over that expected from the Galaxy is seen at lower X-ray energies. The differential absorption at high and low X-ray energies combined with the iron edge energy are strong evidence that partial covering is a crucial determinant of the behaviour observed from Cir X-1. The continuum spectral variability observed by *ASCA* can also be understood naturally in terms of partial covering column changes. There is evidence for a relatively weak emission line from neutral iron with an equivalent width of only about 65 eV. After the flux transition, the strength of the edge feature is greatly reduced, suggesting a large reduction in the amount of partial covering. For a large region of statistically acceptable chi-squared parameter space, the luminosity of Cir X-1, after correction for partial covering, need not change during the transition. We discuss models for the partial covering and suggest that X-ray scattering by electrons may be important. Aspects of the Cir X-1 spectrum are very similar to those of Seyfert 2 galaxies with Compton-thin tori.

Key words: stars: individual: Circinus X-1 – X-rays: stars – stars: neutron.

1 INTRODUCTION

Circinus X-1 (hereafter Cir X-1) is a peculiar and poorly understood X-ray binary with an approximately 16.6 day period in which the compact object is thought to be a neutron star (Tennant, Fabian & Shafer 1986). The neutron star magnetic field strength, companion star spectral type and binary orbital parameters are not well determined. The lack of X-ray pulsations and the presence of type 1 X-ray bursts suggest the neutron star magnetic field strength is less than $\sim 10^{11}$ G, and it has been argued that Cir X-1 may be an ‘atoll’ type X-ray binary with a magnetic field strength of less than $\sim 10^9$ G (Oosterbroek et al. 1995 and references therein). However, the broad band X-ray spectrum of Cir X-1 has been argued to resemble that of a high magnetic field neutron star rather than that of a low magnetic field neutron star (Maisack et al. 1995; compare with Sunyaev et al. 1991), and if Cir X-1 is associated with G321.9 – 0.3

(see Stewart et al. 1993 and references therein) it would perhaps be difficult to understand such a weak magnetic field in such a young neutron star (see figure 1 of Phinney & Kulkarni 1994). Type 1 bursting activity from Cir X-1 appears to be highly intermittent, and to our knowledge no bursts have been seen either before or after the *EXOSAT* series of observations. The optical counterpart to Cir X-1 has been unambiguously identified by Moneti (1992), but reddening uncertainties and potential accretion disc contributions have prevented a precise determination of the spectral type of the companion star. The orbit has been argued to be highly eccentric due to the violent variability seen near zero phase (probably associated with the periastron passage of the neutron star), although proper orbital parameters are lacking. Given the orbital period and claimed space velocity of Cir X-1, it is probable that its orbit was at least initially highly eccentric (see figure 10 of Brandt & Podsiadlowski 1995).

The iron K spectral features of Cir X-1 and their rele-

vance to understanding the X-ray properties of Cir X-1 more generally are also a subject of uncertainty. Very strong and potentially broad iron $K\alpha$ emission lines have been discussed (e.g. Tennant 1985; Miyamoto & Kitamoto 1985; Makino 1993; Gottwald et al. 1995; Maisack et al. 1995), but it is known that complicated iron K spectral features can be difficult to interpret using data with low spectral resolution (e.g. Tennant 1988a; Gottwald et al. 1995). In particular, in Cir X-1 models where a large amount of partial or total covering is present (e.g. Ikegami 1986; section 3.2 of Tennant 1988b; Inoue 1989; section 5 of Oosterbroek et al. 1995), one might expect the presence of a strong iron K edge. In this paper we use the excellent spectral resolution and sensitivity of the Japanese/USA Advanced Satellite for Cosmology and Astrophysics (hereafter *ASCA*; Tanaka, Inoue & Holt 1994) to probe the iron K complex of Cir X-1 near one of its zero phase transitions.

Following section 3 of Stewart et al. (1993) we take the distance to Cir X-1 to be greater than 6.7 kpc. Neither the optical extinction nor the interstellar X-ray column to Cir X-1 are precisely known, but the X-ray column is thought to be about $(1-2) \times 10^{22} \text{ cm}^{-2}$ (e.g. Predehl & Schmitt 1995). We note that significantly smaller X-ray column values and arguments based on them (e.g. section 3 of Stewart et al. 1991) may have trouble explaining the strength of the dust scattering halo of Cir X-1 as shown in figure 7 of Predehl & Schmitt (1995).

In some of the spectral fitting below we shall implicitly assume Morrison & McCammon (1983) abundances (e.g. when we fit cold absorption and partial covering models). To our knowledge there is no evidence which suggests that these abundances are incorrect, and scalings to different abundances may be made from our results.

2 OBSERVATIONS AND DATA REDUCTION

Cir X-1 was observed with *ASCA* during AO-2 on 1994 August 4–5 using both Solid-state Imaging Spectrometer CCD detectors (SIS0 and SIS1) and both Gas Imaging Spectrometer scintillation proportional counters (GIS2 and GIS3). The energy resolutions of the SIS and GIS detectors are ≈ 2 per cent and ≈ 8 per cent at the iron K complex. The observations started at 20:13:09 UT on 1994 August 4 and ended at 10:30:45 UT on 1994 August 5. They covered the time of zero phase as given by equation 1 of Glass (1994) for $N = 392$.

The SIS detectors were operated in 1 CCD mode, and the most well-calibrated SIS chips were used (chip 1 for SIS0 and chip 3 for SIS1). Bright mode was used for high bit rate data and fast mode was used for medium bit rate data. We shall use only the bright mode data in this paper, and the telemetry limit is $256 \text{ count s}^{-1} \text{ SIS}^{-1}$ for these data. The telemetry is saturated during the latter part of the observation, and we only analyze the SIS data for which the telemetry is not saturated. Cir X-1 was placed at the nominal 1 CCD mode pointing position.

The GIS were operated in PH mode, and the bit assignment was changed so as to give 6 bits of X and Y positional information and an extra 4 bits of timing information (10-6-6-5-0-4 in the notation of section 3.3 of Day et al. 1995b). We thus obtain 64×64 pixel images (i.e. *RAWXBINS*

and *RAWYBINS* each have the value 64; note however that the GIS field of view is circular) and 1024 channel energy spectra in the 1–10 keV band. The telemetry limit is 128 and $16 \text{ count s}^{-1} \text{ GIS}^{-1}$ for the high and medium telemetry bit rates, respectively. The telemetry was completely saturated for the medium bit rate data, and was saturated for the latter part of the observation even at high bit rate. We shall use only the high bit rate data in this paper. When GIS photons are lost due to telemetry saturation, they are lost in a way that leaves the spectral shape unaffected. Thus GIS data that suffer from telemetry saturation can be analyzed reliably after suitable corrections (see below).

We have used the ‘Revision 1’ processed data from Goddard Space Flight Center (GSFC) for the analysis below (Day et al. 1995a), and data reduction was performed using *FTOOLS* and *XSELECT* (see Day et al. 1995b for a description of these packages and their application to *ASCA* data analysis). In this paper we focus on the iron K spectral features observed from a very bright source, and we have chosen our basic data screening criteria after consultation with the GSFC *ASCA* help service. The basic screening criteria we adopt in this paper are listed in Table 1. We have used the *SISCLEAN* and *GISCLEAN* software in *FTOOLS* as appropriate, and for the SIS detectors we only use event grades 0, 2, 3 and 4.

The *ANG-DIST* housekeeping parameter is unacceptably large for the first ≈ 1500 s of the observation as expected, but then it remains within the criteria of Table 1.

3 ANALYSIS

We first extracted images for Cir X-1 in each detector and examined them. At low energies the profile of Cir X-1 has extent over that expected for a point source due to its dust scattering halo (see Predehl & Schmitt 1995 for a detailed study of the dust scattering halo using higher spatial resolution data from the *ROSAT* PSPC). This dust halo will seriously hinder X-ray imaging searches for jet emission. At higher energies (above ≈ 5 keV), the profile of Cir X-1 is consistent with that of a point source (this is as expected since dust scattering halo intensities drop strongly with increasing energy; see section 3.6 of Predehl & Schmitt 1995). There are no other strong X-ray sources in the fields of view. However, the GIS detectors also show weak apparent emission to the south of Cir X-1 at their edges (this emission is not from the calibration sources). This ‘shoulder-like’ emission is part of the point spread function and is common in observations of bright sources (K. Ebisawa, private communication). We are confident that this emission originates from Cir X-1 and is not from another X-ray source because its variability tracks the variability from Cir X-1 described below (with reduced absolute amplitude).

We use circular source cells centered on Cir X-1 with radii of ≈ 4.5 arcmin and ≈ 9 arcmin for SIS and GIS source count extraction, respectively. The choice of background regions is not straightforward for the SIS detectors. The brightness of Cir X-1 requires us to use small circular regions of radius ≈ 1.2 arcmin near the northeastern (SIS0) and southeastern (SIS1) chip corners. Even with these regions, there is still some contribution from Cir X-1 to the background cells. For the GIS detectors we use circular back-

Table 1. Data screening criteria for the SIS and GIS detectors. Details on these screening criteria may be found in section 5.2 of Day et al. (1995b).

SIS screening criteria	GIS screening criteria	Description
SAA= 0	SAA= 0	Only use data taken outside the South Atlantic Anomaly (boolean variable)
ELV> 5	ELV> 5	Earth elevation angle for target (degrees)
COR> 4	COR> 4	Minimum cut-off rigidity ($\text{GeV } c^{-1}$)
ANG_DIST> 0.0	ANG_DIST> 0.0	Angular distance of field of view from specified direction (degrees)
ANG_DIST< 0.01	ANG_DIST< 0.01	Angular distance of field of view from specified direction (degrees)
T_SAA< 0 or T_SAA> 16	—	Avoid high background data just after SAA passage (seconds)
SO_PIXL1> 0	—	Number of events detected by chip 1 above the event threshold (SIS0 only)
SO_PIXL1< 400	—	Number of events detected by chip 1 above the event threshold (SIS0 only)
S1_PIXL3> 0	—	Number of events detected by chip 3 above the event threshold (SIS1 only)
S1_PIXL3< 400	—	Number of events detected by chip 3 above the event threshold (SIS1 only)
—	G2_L1> 0.0	Only use data inside the PHA discriminator range (GIS2 only)
—	G3_L1> 0.0	Only use data inside the PHA discriminator range (GIS3 only)

ground cells with radii of ≈ 2.0 arcmin that are essentially free of emission from Cir X-1. We have found that different background regions have very little effect on the results of the analysis presented below.

3.1 Variability near zero phase

3.1.1 Count rate variability

Source and background light curves were extracted for all instruments. We have corrected the GIS light curves for dead time effects by multiplying each point by the (time varying) factor $1/(1-\text{G2_DEADT})$ for GIS2 and $1/(1-\text{G3_DEADT})$ for GIS3. The G2_DEADT and G3_DEADT parameters are obtained from the *ASCA* housekeeping file, and they include the effects of both instrumental and telemetry dead time. When we quote GIS count rates below we implicitly include the correction for detector dead time. We found good general agreement between the shapes of the source light curves. There was also good general agreement between the shapes of these light curves and the shapes of the G2_L1 and G3_L1 light curves. There is no evidence for strong background flaring, even when the screening criteria shown in Table 1 are neglected (variability in the SIS background light curves can be attributed to the small contamination from Cir X-1 itself).

In Figure 1 we show the screened GIS2 light curve of Cir X-1 in the 1–10 keV band. Cir X-1 is in a relatively low count rate state ($\approx 30 \text{ count s}^{-1}$) for about 6000 s, and it then makes an abrupt transition to a state where the mean GIS count rate is a factor of ~ 10 times higher. Given the detector position of Cir X-1, it has a GIS count rate of about 0.05 times that of the Crab during the low count rate state and a GIS count rate of about 0.55 times that of the Crab during the high count rate state. The high count rate state shows strong and rapid variability for its first ≈ 6000 s, but Cir X-1 then settles into a calmer mode of behaviour. The Eddington limit of Cir X-1 for hydrogen-poor material is thought to correspond to a flux of about $2.4 \times 10^{-8} \text{ erg cm}^{-2} \text{ s}^{-1}$ (see section 2 of Stewart et al. 1991 but be wary of partial covering effects as described below), and in the high count rate state the flux after correction for only Galactic absorption is comparable to the Eddington limit flux (see Table 2 for numerical flux values).

The basic shape of the zero phase light curve has been seen to change greatly over the years (see the discussion in section 3 of Tennant 1988b and Whitlock & Tyler 1994). Our observations do not show evidence for basic shape changes from the *GINGA* all-sky monitor and pointed observations reported by Tsunemi et al. (1989) and Makino (1993), although the rise after zero phase may be to a somewhat lower level^{*}. We have verified this via further examination of the unpublished *GINGA* all-sky monitor data which show that Cir X-1 does not appear to significantly exceed 1.3 Crab in the 1–20 keV band during 1987–1992 (note that the ‘1.8’ and ‘0.6’ in the caption for figure 8 of Tsunemi et al. 1989 are incorrectly transposed; see figure 7 of Tsunemi et al. 1989 and H. Tsunemi, private communication). *RXTE* all-sky monitor observations from 1996 show flux dips before zero phase as well as flux rises up to a remarkable 2–3 Crab shortly after (within about 0.2–0.6 days) zero phase (see Shirey et al. 1996). It is hard to determine whether the data from the *GINGA* all-sky monitor or the *RXTE* all-sky monitor are more germane for comparison with our 1994 *ASCA* data, although we do not see evidence for a count rate rise as dramatic as is now seen by *RXTE*. In any case, we note that the observed variability supports the discussion in section 3 of Glass (1994) regarding ephemerides.

The high count rate state variability at 28000–36000 s in Figure 1 is of concern since the two rises appear to have similar shapes. We have manually examined the ANG_DIST parameter during this time, and while small fluctuations of ≈ 9 arcsec or less are present, they do not appear to be able to explain the variability. This variability is also seen in the G2_L1, G2_LDHI, G3_L1 and G3_LDHI housekeeping parameters, and the G2_H0, G2_H2, G3_H0 and G3_H2 housekeeping parameters appear to be reasonably behaved during

^{*} We also made *ASCA* observations of Cir X-1 on 1994 August 26. These observations are about 5 days past zero phase according to equation 1 of Glass (1994) for $N = 393$, and the observed mean GIS2 count rate is $\approx 350 \text{ count s}^{-1}$ with ≈ 10 per cent variability. Comparison of this fact with Figure 1, figure 1 of Tennant (1988a), figure 8 of Tsunemi et al. (1989) and *RXTE* all-sky monitor data suggests that the ‘decay’ of the flux from Cir X-1 after zero phase may be progressively occurring less rapidly. Further observations to search for such trends are needed.

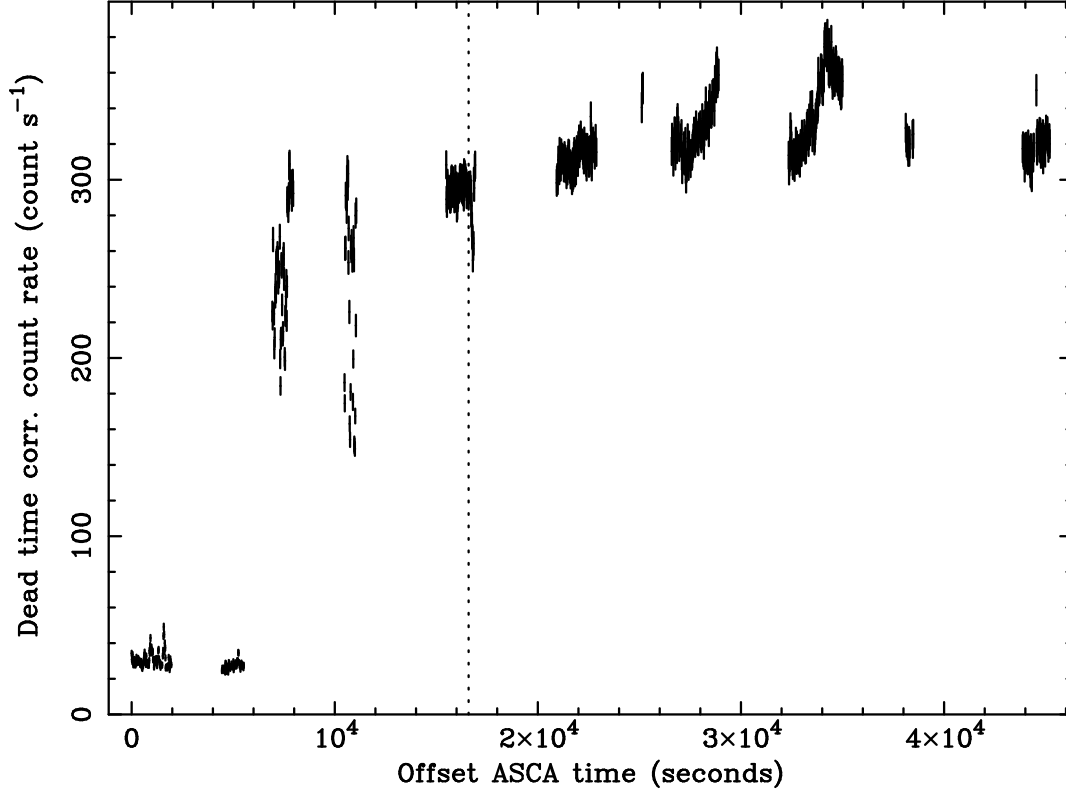


Figure 1. Screened *ASCA* GIS2 light curve of Cir X-1 after correction for detector dead time (see the text for the correction method used). The light curve is for the energy band 1.0–10.0 keV (GIS channels 85–849). The abscissa is in seconds after 20:37:12 UT on 1994 August 4, and the data point bin size is 16 seconds. The vertical dotted line shows the predicted time of zero phase from equation 1 of Glass (1994) with $N = 392$. We shall refer to the first 6000 s of data as the ‘low count rate state’ and the data after this time as the ‘high count rate state.’ There is very rapid and large amplitude variability between 6000–12000 s, and this variability causes the rough appearance of the data in this time interval.

this time. The cut-off rigidity is well above 4 GeV c^{-1} during this time.

3.1.2 Spectral variability

In Figure 2 we show GIS2 hardness ratios as a function of time. We define HR1 to be the ratio of the count rate in GIS2 channels 256–849 to that in channels 85–255 (these energy ranges approximately correspond to 3.0–10.0 keV and 1.0–3.0 keV). We define HR2 to be the ratio of the count rate in GIS2 channels 171–255 to that in channels 85–170 (these energy ranges approximately correspond to 2.0–3.0 keV and 1.0–2.0 keV). We define HR3 to be the ratio of the count rate in GIS2 channels 426–849 to that in channels 256–425 (these energy ranges approximately correspond to 5.0–10.0 keV and 3.0–5.0 keV). Note that we have reduced the length of the abscissa of Figure 2 relative to that of Figure 1 to only show the period of strongest spectral variability.

During the low count rate state (the first 6000 s of Figure 2) Cir X-1 shows strong HR1 and HR3 variability but much less HR2 variability. The HR1 and HR3 variability often has a flare-like character. The HR2 data during the low count rate state can be fit acceptably with a constant value

of 0.969 ($\chi^2_\nu = 0.97$ for 181 degrees of freedom), although there do appear to be some small systematic residuals. In light of this result we have examined the 1.0–3.0 keV light curve, and during the low count rate state the variability in this band is much less than that at higher energies. While the data are not strictly consistent with a constant model ($\chi^2_\nu = 1.17$ for 181 degrees of freedom), no systematic count rate fluctuations by more than 20 per cent from the mean are apparent. In addition, the flare-like behaviour seen at higher energy is not obviously visible below 3 keV.

All three hardness ratios are seen to change significantly after the transition from the low count rate state to the high count rate state, although the change at high energies appears to be less than that at low energies.

After 12000 s (not shown in Figure 2), much less hardness ratio variability is seen. In particular, there is no apparent spectral variability corresponding to the count rate variability seen in Figure 1 between 28000–36000 s. Statistical analysis shows that there is a slow general decline of at least HR1 and HR3 with time. HR1 declines from 1.33 to 1.22, and HR3 declines from 0.46 to 0.44.

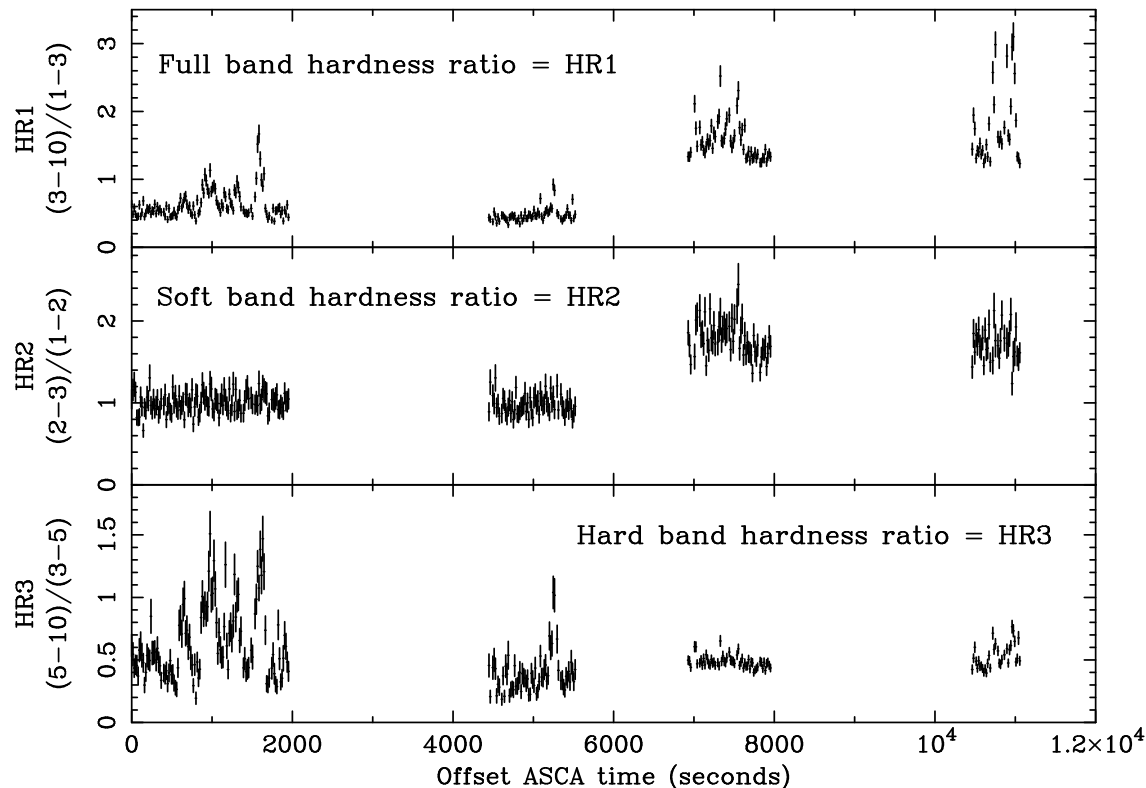


Figure 2. *ASCA* GIS2 hardness ratios of Cir X-1 as a function of time. The ordinate labels denote energy ranges in keV. The abscissa offset is the same as that for Figure 1, and we have only shown the start of the observation where the strongest spectral variability is observed. The data point bin size is 16 seconds. Note that HR3 can vary strongly while HR2 remains constant.

3.2 Spectra near zero phase

Our *ASCA* observation provides the highest spectral resolution view of Cir X-1 yet possible and allows a sensitive probe of its iron K spectral features. To model the continuum underlying these features, we have used a two blackbody model. As we shall show below, this model fits the continuum in the *ASCA* band well even if the fitted blackbody parameters may not have precise translations into physical quantities. This continuum model was also found to fit the broader band (≈ 2 –25 keV) and very high statistical quality *GINGA* data the best (Makino 1993). We have verified that our conclusions regarding the iron K spectral features are not materially altered if we use different continuum models such as Comptonized blackbodies (this is due to the good spectral resolution and good statistics). In addition, if we ignore the data below 3 keV and just use a power law to fit the 4–10 keV data our results are not qualitatively changed. In all fits below we include the effects of interstellar absorption. In our fits with partial covering we, of course, take the interstellar absorption to be unaffected by the partial covering.

Photon pile-up effects are a concern for *ASCA* SIS observations of bright sources (see Ebisawa et al. 1996 for a detailed discussion of this issue). Cir X-1 has a mean count rate during the low count rate state of $\approx 30 \text{ count s}^{-1} \text{ SIS}^{-1}$, and

photon pile-up effects are unlikely to compromise the analysis below. We have used ring-shaped extraction regions to verify that our results are not strongly influenced by photon pile-up effects. We note that the pile-up spectrum is smooth (see figure 11 of Ebisawa et al. 1996) and cannot falsely imprint the sharp spectral features we describe below.

We use the SIS redistribution matrix files (rmf) from 1994 Nov 9 and the GIS rmf from 1995 March 6. We generate our ancillary response files (arf) using the *ASCA*ARF software. We have used the *DEADTIME* program in *FTOOLS* to correct for dead time effects. We model the X-ray spectra of Cir X-1 using the X-ray spectral models in the *XSPEC* spectral fitting package (Shafer et al. 1991).

3.2.1 Low count rate state spectral fitting

Average spectral properties

In order to obtain a ‘first look’ at the spectrum in the low count rate state, we have binned spectra for all four detectors using all of the low count rate state data. We group these spectra so that there are at least 20 photons per spectral data point (we shall implicitly adopt this grouping for all spectra below unless stated otherwise). Figure 2 shows that there is significant spectral variability within the low count rate state, and thus these spectra must be regarded to be

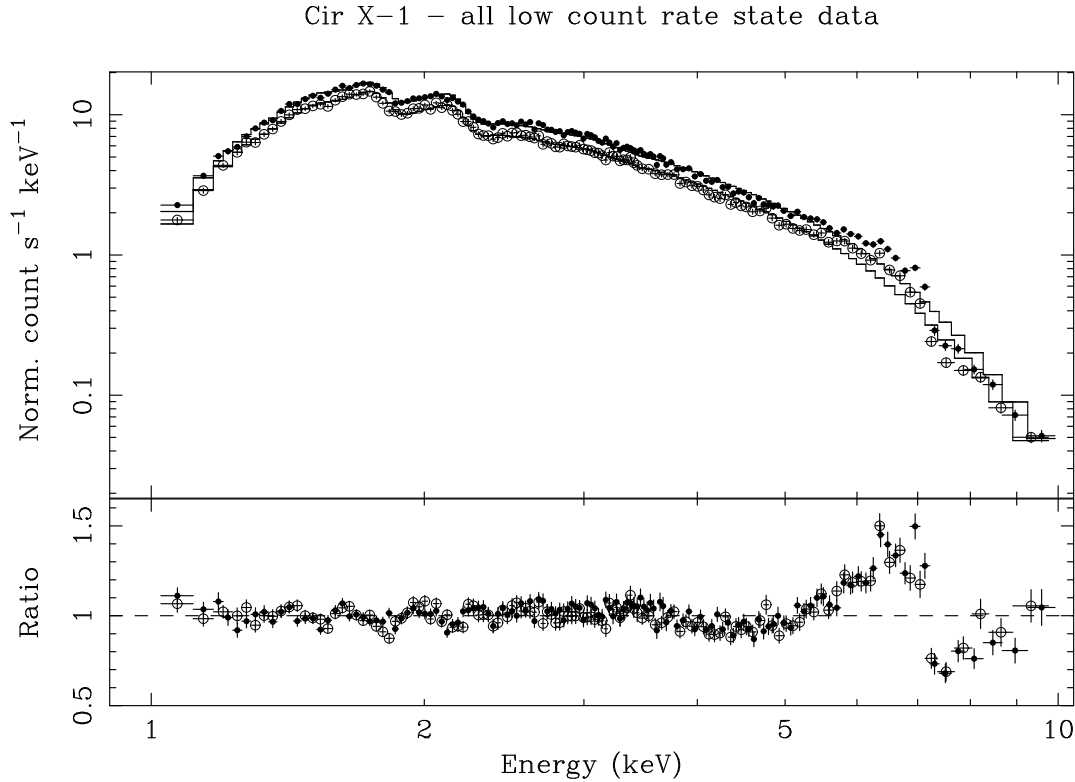


Figure 3. Average SIS0 (solid circles) and SIS1 (open circles) spectra for the low count rate state data. The best fitting absorbed two blackbody model is shown along with the data-to-model ratio. Note the sharp drop in the data-to-model ratio just above 7 keV. The SIS detector resolution at the iron complex is about 140 eV, and the shown data points in this energy range are essentially statistically independent. The sharp drop can be interpreted as an iron edge from partial covering.

crude and only meaningful in a time-averaged sense. However, the excellent statistics afforded by this first look give useful insight. We note that an unlikely conspiracy would be required for spectral variability effects to produce sharp spectral features at the energies of known strong atomic features.

In Figure 3 we show average SIS0 and SIS1 spectra for the entire low count rate state. The two spectra agree well in shape, and the GIS2 and GIS3 spectra are consistent with those in Figure 3 (they are not displayed only for reasons of clarity). We have used the two blackbody model with simple cold absorption (see above) to fit these data, and we show the ratio of the data to the best fitting model. In this fitting the blackbody normalizations are all taken to be free parameters, but the other spectral parameters are tied together (we adopt this fitting prescription for all fits below unless stated otherwise). The most noticeable feature in the ratio plot is the large and sharp drop just above 7 keV. A natural interpretation for this drop is that it is due to an absorption edge from a large column of neutral or nearly-neutral iron atoms. The broad 5.3–7.1 keV excess and smaller 3.8–5.3 keV deficit may be understood as statistical artefacts from the fit trying to compensate for the presence of the large edge (fits which include the edge reduce the amplitudes of these features to where they are insignificant,

see below). A large edge from iron would be expected in models for Cir X-1 where a large amount of obscuring matter lies between the X-ray generation region and Earth, and one would not be naturally expected in other models. The iron structure could perhaps also be interpreted as broad iron line emission from matter moving with relativistic speed, and we shall critically examine this possibility below. There is also some secondary residual structure between 6–7 keV, although this structure is not as strong as that just above 7 keV. There are no strong residuals in the 1–3 keV band.

‘Calm’ set of data

In order to probe the spectral properties of the low count rate state in a more precise manner, we have carefully selected a 450 s interval of data where there is relatively little flux and spectral variability. This interval begins at 21:55:31 UT. We have binned spectra for all four detectors and fit these spectra using the two blackbody model with simple cold absorption. We derive the results shown in column 1 of Table 2. This model can be ruled out with greater than 94 per cent confidence, and similar systematic residuals to those shown in Figure 3 are present.

The depth of the putative edge seen in the residuals and in Figure 3 is suggestive of intrinsic absorption by a column of $\sim 10^{24} \text{ cm}^{-2}$ even though we do not see significant ab-

Table 2. Spectral fitting results.

‘CR’ stands for ‘count rate’, ‘PC’ stands for ‘partial covering’ and ‘BB’ stands for blackbody.

The fitting models used below are defined in Shafer et al. (1991). When we fit blackbody models we are using the ‘bbodyrad’ model, and when we fit partial covering models we are using the ‘pcfabs’ model. The blackbody model normalizations (A_1 and A_2) are formally related to the radii of the emission regions, although as commented in the text the derived radii are likely to only be characteristic quantities. A ‘bbodyrad’ normalization is formally equal to the square of the emission region radius in kilometers divided by the square of the distance to Cir X-1 in units of 10 kpc.

The errors for all fits are quoted for 90 per cent confidence, conservatively taking all free parameters to be of interest other than absolute normalization (Lampton, Margon & Bowyer 1976).

Fluxes and normalizations are quoted for SIS0 when possible. When SIS data are not available due to telemetry saturation we quote fluxes and normalizations for GIS2. All fluxes and luminosities are for the 1–10 keV band. When we compute unabsorbed fluxes we remove the effects of both interstellar absorption and intrinsic partial covering.

‘d.o.f.’ stands for ‘degrees of freedom’. The $P(\chi^2 | \nu)$ chi-square probability function is defined in section 6.2 of Press et al. (1989).

Fit parameter name	‘Calm’ low CR state No PC (1)	‘Calm’ low CR state PC on both BB (2)	‘Calm’ low CR state PC on hot BB (3)	HR3> 0.9 low CR state PC on both BB (4)	High CR state No PC (5)	High CR state PC on both BB (6)
Interstellar $N_H/(10^{22} \text{ cm}^{-2})$	$1.77^{+0.11}_{-0.11}$	$1.79^{+0.15}_{-0.12}$	$1.80^{+0.16}_{-0.13}$	$1.82^{+0.23}_{-0.20}$	$1.82^{+0.08}_{-0.08}$	$1.79^{+0.11}_{-0.15}$
kT_1 (keV)	$0.48^{+0.03}_{-0.03}$	$0.46^{+0.03}_{-0.04}$	$0.46^{+0.03}_{-0.04}$	$0.46^{+0.05}_{-0.05}$	$0.59^{+0.03}_{-0.03}$	$0.59^{+0.07}_{-0.05}$
A_1	3710^{+930}_{-710}	$(6.5^{+4.8}_{-4.2}) \times 10^4$	4150^{+1760}_{-1110}	$(4.0^{+2.0}_{-1.2}) \times 10^4$	8950^{+2030}_{-1520}	$(1.5^{+10.5}_{-0.7}) \times 10^4$
kT_2 (keV)	$1.49^{+0.15}_{-0.13}$	$1.16^{+0.19}_{-0.15}$	$1.15^{+0.17}_{-0.15}$	$1.51^{+0.12}_{-0.13}$	$1.42^{+0.03}_{-0.03}$	$1.38^{+0.04}_{-0.05}$
A_2	19^{+6}_{-6}	775^{+980}_{-460}	810^{+2040}_{-600}	201^{+120}_{-68}	565^{+60}_{-63}	1080^{+5120}_{-730}
Partial covering percentage	—	$93.8^{+4.8}_{-10.6}$	$93.8^{+4.7}_{-10.8}$	$89.6^{+5.0}_{-5.1}$	—	42^{+54}_{-31}
Partial covering $N_H/(10^{22} \text{ cm}^{-2})$	—	162^{+44}_{-41}	161^{+104}_{-58}	42^{+7}_{-6}	—	123^{+109}_{-108}
Absorption uncorrected flux/ $(10^{-9} \text{ erg cm}^{-2} \text{ s}^{-1})$	1.5	1.5	1.5	3.5	24	24
Absorption corrected flux/ $(10^{-9} \text{ erg cm}^{-2} \text{ s}^{-1})$	2.5	38	16	25	33	41
χ^2	1001	931.6	931.3	1075	1389	1364
d.o.f.	932	930	930	1079	1279	1277
χ^2_ν	1.074	1.001	1.001	0.996	1.086	1.068
$P(\chi^2 \nu)$ rejection probability (if significant)	94.2	—	—	—	98.3	95.5

sorption over the expected Galactic value at lower X-ray energies. This large differential column could either be explained by partial covering from thick matter or by absorption from ionized matter. Due to the fact that the putative edge energy corresponds to that of neutral or nearly-neutral iron, partial covering seems more plausible than warm absorption. If we include partial covering of both blackbodies, we derive the results shown in column 2 of Table 2. The fit is statistically very good. In Figure 4 we show partial covering chi-squared contours for this fit as the solid set of contours. Note that a very large partial covering fraction is required by these data and that as a result the partial covering corrected isotropic luminosity for the low count rate state is

of order the Eddington luminosity (it is difficult to be more specific than this because the observed X-ray bursts could have been affected at some level by partial covering too).

Narrow emission lines from iron have been seen in X-ray binaries (e.g. Ebisawa et al. 1996), and Figure 3 suggests the presence of an emission line from neutral or nearly-neutral iron. We have thus added a 6.40 keV (see House 1969) Gaussian emission line with $\sigma = 10$ eV to our fit. This addition gives $\chi^2 = 924.3$ for 929 degrees of freedom, a significant improvement (the other fit parameters are not changed significantly by the addition of the line). Adding narrow lines at other energies (e.g. 4.0 keV, 6.1 keV, 6.6 keV) does not improve the fit significantly. The line flux is $(8.9^{+8.9}_{-5.6}) \times 10^{-3}$

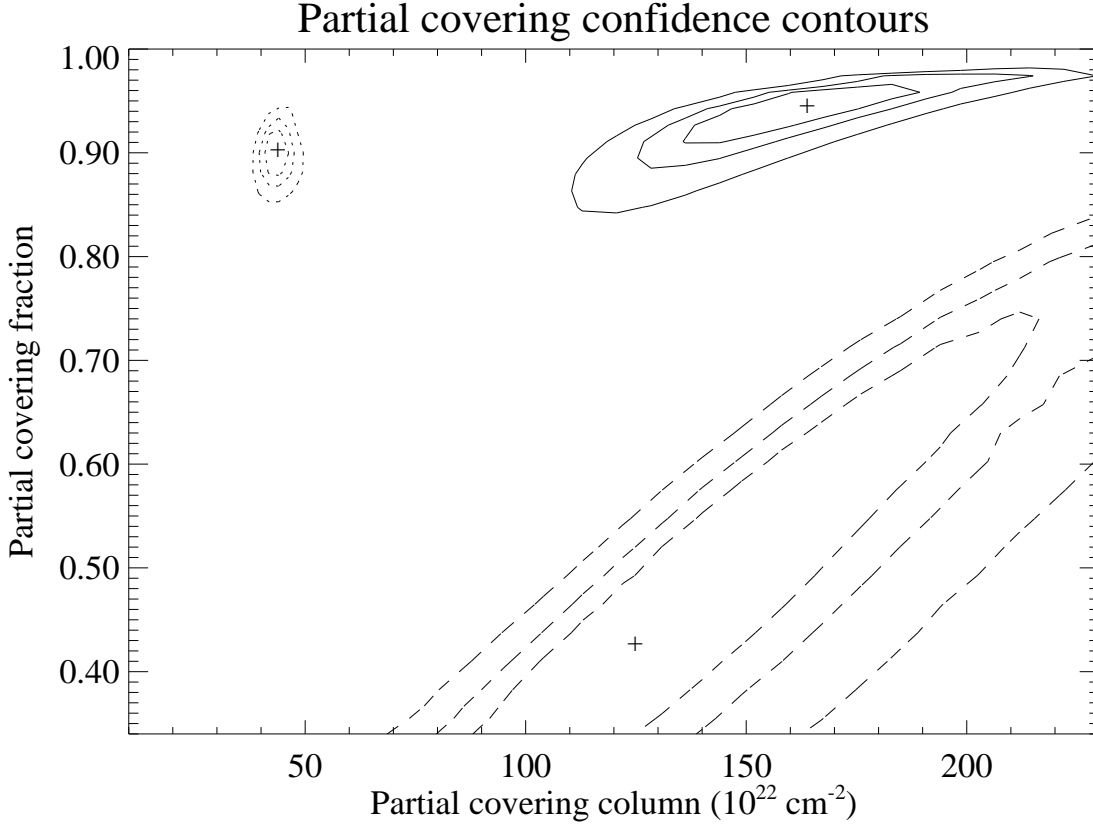


Figure 4. Contours of the partial covering model for the ‘calm’ low count rate state data (solid curves near upper right), the low count rate state data with HR3 greater than 0.9 (dotted curves near upper left) and the high count rate state data (dashed curves). The partial covering is taken to affect both blackbodies (see the text). Contour levels for each set are for $\Delta\chi^2 = 2.30$ (68.3 per cent confidence for two parameters of interest), $\Delta\chi^2 = 4.61$ (90.0 per cent confidence for two parameters of interest) and $\Delta\chi^2 = 9.24$ (90.0 per cent confidence for five parameters of interest). Crosses show the best fit values. The low count rate state contours have been made using data from all four *ASCA* detectors, while the high count rate state countours have been made only using data from the GIS detectors. The partial covering luminosity correction increases towards the upper part of this diagram, especially for partial covering fractions near unity.

photons $\text{cm}^{-2} \text{s}^{-1}$, and the line equivalent width is 65^{+66}_{-41} eV (these errors are for $\Delta\chi^2 = 2.71$). The equivalent width we obtain from fitting the data shown in Figure 3 is comparable to this value. While there may also be small 6.7–6.9 keV lines from ionized iron, we are not able to formally prove the existence of such lines. The other detectors do not have ≈ 6.9 keV residuals as strong as the SIS0 ≈ 6.9 keV point shown in Figure 3.

We have also considered the possibility that only the higher temperature blackbody component suffers from partial covering. While figure 4 of Inoue (1989) appears to be at odds with this possibility, we note that HR2 does not vary during the low count rate state while HR3 does. The absence of HR2 variability, the absence of large 1.0–3.0 keV count rate variability (see above) and the presence of HR3 variability could be suggestive of partial covering interposed between the higher and lower temperature blackbody emission regions (but see our further discussion of this issue below in the context of partial covering column changes). From our fitting we derive the results shown in column 3 of Table 2. This is also a statistically good fit and thus from model fitting alone we cannot clearly determine whether the partial covering affects both blackbodies or only the

higher temperature one. If we make partial covering contours such as those shown in Figure 4, they look very similar to the solid ones already shown. If we use the low and high temperature blackbody normalizations and a distance of 6.7 kpc to derive crude blackbody radii, the higher temperature blackbody has a radius of $\lesssim 36$ km and the lower temperature blackbody has a radius of $\lesssim 52$ km. Thus in this scenario the matter doing the partial covering would be roughly ~ 40 km from the neutron star. A very large density of $\gtrsim 10^{22} \text{ cm}^{-3}$ would be required for iron to be nearly neutral, as implied by the energy of the iron edge (see Ross 1978 and Kallman & McCray 1982). This density is remarkably high, being ~ 1400 times larger than the Eddington number density for accretion onto a $1.4 M_{\odot}$ neutron star ($n_{\text{Edd}} = L_{\text{Edd}}/4\pi r_g^2 c^3 m_p = 10^{19} (M/M_{\odot})^{-1} \text{ cm}^{-3}$ where $r_g = GM/c^2$; see appendix C of Phinney 1983 and compare this density with section 5.6 of Frank, King & Raine 1992). The presence of such a dense partial coverer would be difficult to understand. Thus partial covering of just one blackbody, while statistically acceptable, does not appear to be physically plausible. The lack of strong Doppler blurring of the edge may also suggest that the partial coverer is significantly further than ~ 40 km from the neutron star. If the

partial covering affects both blackbodies, we derive a radius for the lower temperature blackbody of ~ 170 km, and the partial coverer could be far outside this radius. Thus scenarios in which the partial covering affects both blackbodies significantly alleviate the density contrast problem.

Now we consider the possibility that the iron K residuals are primarily due to a broad iron emission line from matter moving with relativistic speed near the neutron star (e.g. Brandt & Matt 1994 calculate the expected iron $K\alpha$ line properties from matter in an ionized accretion disc around a neutron star). The blue horns of such lines can sometimes drop quite sharply at their high energy ends, and this could perhaps produce the sharp drop shown in Figure 3. We have fit the XSPEC ‘diskline’ model to the iron K spectral features. This model includes Doppler, transverse Doppler and gravitational redshift effects but does not include light bending (Fabian et al. 1989 describe the physics used in the ‘diskline’ model but note that not all of the physics discussed in Fabian et al. 1989 is actually implemented in the model). We constrain the line rest energy to be in the range 6.40–6.97 keV (this is the iron K line energy range from House 1969 and Ross 1978). We fix the disc inner radius to be $6r_g$ and constrain the disc outer radius to be larger than $7r_g$. We have found that the statistically best fits are obtained when we use the special ‘10’ disc emissivity law appropriate for a black hole disc (see Shafer et al. 1991 and the XSPEC ‘diskline’ code). In this fit the line energy rises to 6.97 keV and the inclination drops to 0 degrees. The best fitting disc outer radius is $110r_g$, but this parameter is poorly constrained by these data. The line equivalent width is 440 eV. This equivalent width, while large, is perhaps not impossible for an ionized accretion disc (e.g. Matt, Fabian & Ross 1993). The fit gives $\chi^2 = 943.4$ for 928 degrees of freedom, and is thus statistically acceptable. From examination of the best fitting line model, it is apparent that the high energy drop of the blue horn of the line mimics the effect of an edge, as discussed above. We note that while a relativistic line cannot be formally falsified with these data, partial covering provides a slightly smaller χ^2 with fewer free parameters ($\Delta\chi^2 = 11.8$ with 2 fewer parameters). In particular, the drop just above 7 keV is uniquely and naturally specified in the partial covering model by the edge energy of cold iron. In addition, aspects of the observed spectral variability and low-to-high count rate state transition can be best explained in terms of partial covering (see below).

In light of the results of this section, it appears likely that some earlier and lower spectral resolution observations which modeled the iron K complex of Cir X-1 with only a line feature were not entirely correct.

Other sets of data

We have also fit other sets of data to investigate the extent to which our discussion above is generally applicable to the low count rate state. The first 500 s of data in Figure 1 show relatively little flux and spectral variability, and the spectral residuals from these data are consistent with those discussed above. If we fit a partial covering model to these data, we obtain a set of contours that is very similar to the solid set shown in Figure 4. The partial covering fraction is again required to be greater than 80 per cent with very high statistical significance.

Unfortunately, there are no other contiguous sets of low

count rate state data during which both HR1 and HR3 remain well-behaved for 200 s or more (200 s is about the time required to obtain a high quality spectrum during the low count rate state). In order to proceed further, we are forced to mollify our rigorous prescription of only looking at contiguous data sets with minimal spectral variability. We have selected a set of low count rate state data for analysis during which HR3 is larger than 0.9. The data used were chosen from that taken between 800–1700 s in Figure 2, and the total integration time was 280 s. Our choice of these data allows us to examine a significantly different HR3 range from that examined so far. In Figure 5 we illustrate the difference between a spectrum extracted from these data and one from the ‘calm’ data described above. As one would expect from Figure 2 and its accompanying discussion, the spectra agree well below 3 keV but are very different at higher energies. If, as argued above, the partial covering affects both blackbodies, the excellent agreement below 3 keV rules out any significant changes in the partial-covering fraction between the two data sets. However, the agreement does *not* rule out changes in the partial-covering column density between the two data sets as long as the column remains so high that it always entirely blocks the < 3 keV X-rays that strike it. In fact, the qualitative behaviour shown in Figure 5 is exactly what one would expect from a thick partial covering column that changes with time (this can be understood by examining XSPEC partial covering models with partial covering columns between $5 \times 10^{23} \text{ cm}^{-2}$ and 10^{25} cm^{-2}). If we fit the spectra from all four detectors with only a two blackbody model, the fit is very poor and can be rejected with greater than 99 per cent confidence. If we add partial covering, we obtain a good fit as shown in column 4 of Table 2. We note that the low energy spectral parameters (N_H , kT_1 and A_1) and the partial covering fraction agree well with what was derived for the ‘calm’ set of low count rate state data. While the kT_2 and A_2 contours do not quite overlap with those derived for the ‘calm’ data, they are not strongly different and small discrepancies may be explained by the fact that we have fit a set of data which includes HR3 spectral variability. However, the most noticeable change from the ‘calm’ data set is the strong change in fitted partial covering column. This can be clearly seen by comparison of the dotted and solid contours in Figure 4. The dotted contours are smaller than the solid contours because lower energy photons are now able to penetrate the column and thereby better constrain the fit.

We have also examined other sets of data with HR3 between 0.6–0.9. When we make partial covering contours for these data sets, the contours lie between the dotted and solid sets of contours in Figure 4. These data sets all have partial covering fractions larger than 0.8 with high statistical significance. When we plot them in Figure 5 they lie in between the two curves shown (i.e. the spectrum ‘unzips’ from high to low energy as the partial covering column decreases).

Physically, a large change in the partial covering column without some change in the partial covering fraction would appear somewhat surprising. Below we shall discuss ways in which the apparent partial covering column might change without an accompanying change in the apparent partial covering fraction. We shall also discuss how one might observe apparent partial covering effects from an object as small as a neutron star and its inner accretion disc.

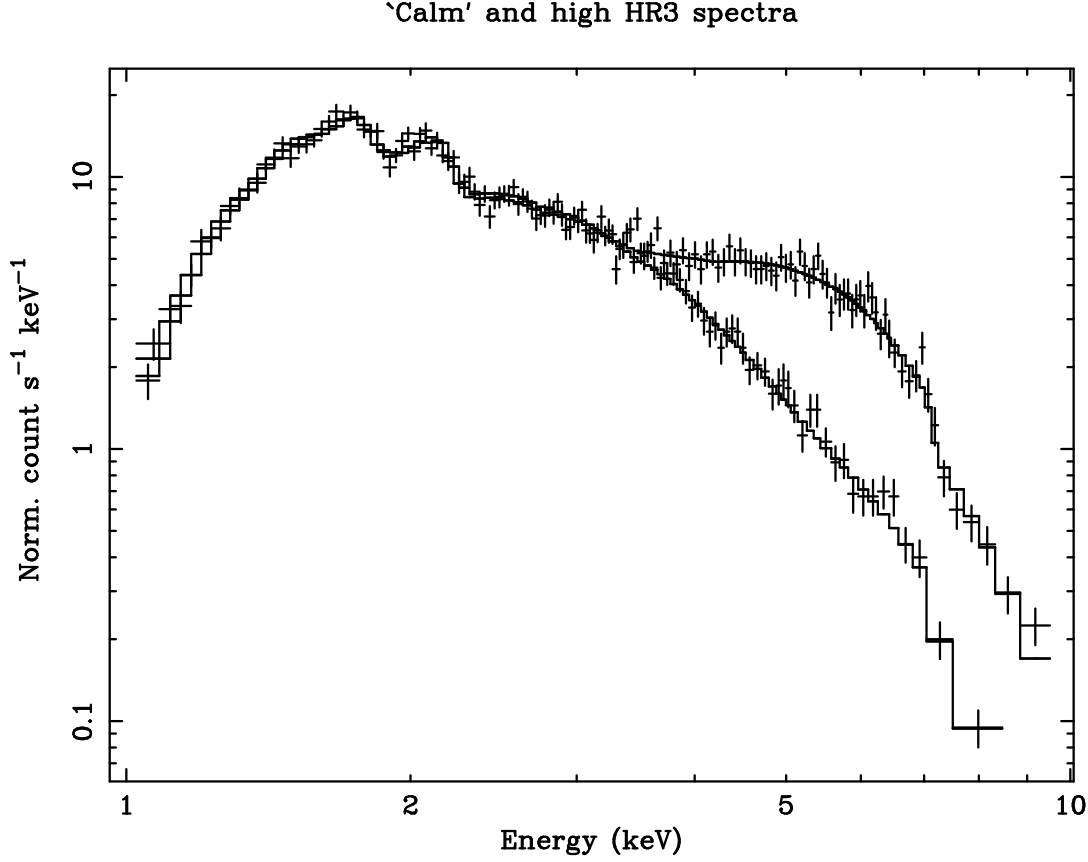


Figure 5. SIS0 spectra extracted from the ‘calm’ set of data (lower spectrum) and a set of data which has HR3 greater than 0.9 (upper spectrum). Note that the spectra agree very well up to about 3 keV but then differ strongly at higher energies. The data sets have been fitted with double blackbody models which include partial covering (see the text). A partial-covering column change can explain the difference between these two spectra (see the text).

3.2.2 High count rate state spectral fitting

Due to telemetry saturation during the high count rate state, we have only been able to perform reliable analyses using the GIS detectors. To begin, we have extracted GIS spectra using only data taken within the 20000–24000 s interval of Figure 1. We group these spectra so that there are at least 40 photons per spectral data point. During this interval there is no strong spectral variability and the flux variability is rather small as well. If we fit the two blackbody model with simple cold absorption to these data, we obtain the results shown in column 5 of Table 2. While this fit is statistically unacceptable and can be rejected with greater than 98 per cent confidence, examination of the data-to-model ratio reveals that fractional deviations from the model are much smaller in the high count rate state than the low count rate state. This important result is illustrated in Figure 6 where we compare data-to-model ratios for the high and low count rate states. The difference in statistical fit quality is thus primarily due to the much larger number of photons available for spectrum construction during the high count rate state. Scrutiny of the high count rate state residuals requires caution due to the fact that any systematic residuals are so small that calibration uncertainties may have non-negligible effects on their interpretation (see appendices A

and B of Ebisawa et al. 1996). Careful examination suggests that there may be a weak edge-like residual present around 7 keV, and this seems at least plausible in light of our results from the previous section. If we add partial covering to our model as per the previous section, we obtain the results shown in column 6 of Table 2. The addition of partial covering gives a significant reduction of χ^2 , although the fit is still not formally acceptable. There are no systematic trends in the residuals that are obviously suggestive of spectral features, and we suspect that calibration uncertainties are contributing significantly to the χ^2 value due to the very good statistics. If we include 2 per cent calibration uncertainties when we bin our spectra (see Tashiro et al. 1995 for a discussion of GIS calibration uncertainties), we are able to obtain statistically acceptable χ^2 values. In Figure 4 we show partial covering confidence contours as the dashed set of contours. The high count rate state contours in this diagram are larger due to the fact that the strength of the residuals that constrain the partial covering are much smaller (see Figure 6). We note that GIS calibration uncertainties almost certainly cannot make the low and high count rate state contours in Figure 4 consistent with each other (as is to be expected from Figure 6).

We have examined whether a narrow 6.4 keV emission line from iron is present in the high count rate state data

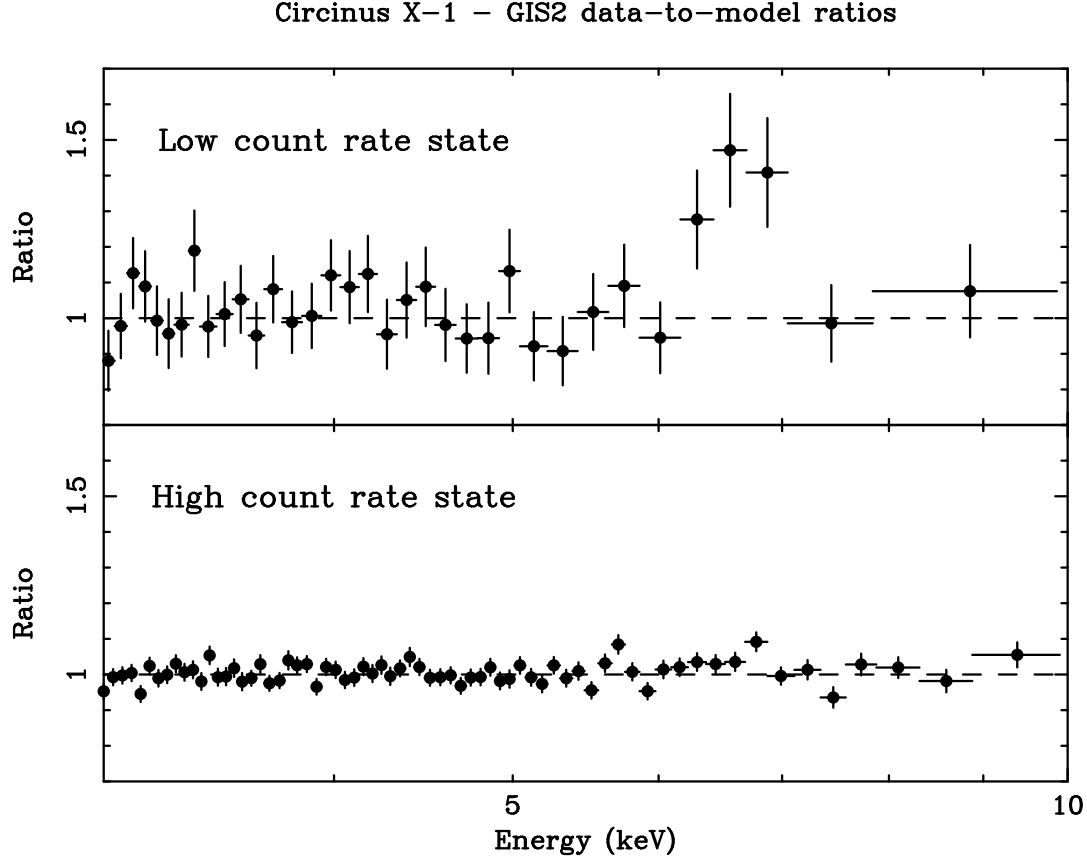


Figure 6. GIS2 data-to-model ratio plots for the low count rate state data (upper panel) and the high count rate state data (lower panel). Note that the abscissae and ordinates of both panels have the same scales, and that the low count rate state data have much stronger iron K complex residual structure than the high count rate state data. The spectral resolution of the data in this figure is about 4 times less than that in Figure 3.

by adding a Gaussian emission line model. The addition of the line is not statistically significant, and the best fitting line normalization is zero. The line normalization can be constrained to be less than 4.5×10^{-3} photons $\text{cm}^{-2} \text{s}^{-1}$ with 90 per cent confidence ($\Delta\chi^2 = 2.71$). This corresponds to a line equivalent width of less than 10 eV. While we find that the line equivalent width is much smaller than for the low count rate state, we cannot formally prove that the line normalization is much smaller.

We have analyzed other sets of data taken after 12000 s in Figure 1, and the iron edge appears to be generally much weaker during this time than during the low count rate state. In particular, spectra created from data taken during the two rises between 28000–36000 s in Figure 1 do not show iron K residuals any stronger than in the bottom panel of Figure 6.

3.2.3 Spectral ratios

As discussed by Inoue (1989), the ratio of two spectra that differ only in the fraction of thick partial covering imposed on them gives useful information about this partial covering. At X-ray energies of < 3 keV, where photoelectric absorption blocks all X-rays striking the partial covering material, the spectral ratio should approach a constant value. This

constant value gives the relative partial covering fractions in the two spectra. At higher X-ray energies, as photoelectric absorption becomes progressively less important, the spectral ratio should approach unity (this effect will not be observable in the *ASCA* band for columns significantly larger than $\sim \sigma_T^{-1} \sim 1.5 \times 10^{24} \text{ cm}^{-2}$). Exactly this behaviour was reported by Inoue (1989), and we have made ratios of our spectra to look for it.

We have made a ratio of the GIS2 spectrum from the ‘calm’ set of low count rate state data to the GIS2 spectrum from the bottom panel of Figure 6 (‘spectral ratio 1’ or ‘SR1’) as well as a ratio of the GIS2 spectrum from the HR3 > 0.9 set of low count rate state data to the GIS2 spectrum from the bottom panel of Figure 6 (‘spectral ratio 2’ or ‘SR2’). We show a plot of these ratios in Figure 7. SR2 starts to approach unity above 4 keV as its numerator’s column is progressively penetrated by higher energy X-rays, and SR1 also starts to rise at the high energy end of the *ASCA* band (this behaviour will be able to be probed much better with *RXTE*). The < 3 keV behaviours of SR1 and SR2 are quite similar. However, these behaviours are both significantly different from that shown in Figure 4 of Inoue (1989). They resemble more closely the behaviour seen by Ikegami (1986). Neither spectral ratio is approximately constant below 3 keV as would be expected under the hy-

pothesis of only a partial covering fraction change between the low count rate state and the high count rate state.

Using the two blackbody continuum model with partial covering, we have also determined that the combination of a partial covering fraction change and a partial covering column change cannot, by itself, explain the difference between the low and high count rate state spectra. We have done this by jointly fitting the GIS spectra for the ‘calm’ low count rate state data and the high count rate state data. In this fitting we tie all model parameters together other than those of the partial covering. The GIS2 and GIS3 blackbody normalizations are separately tied together for each pair of spectra. We include 2 per cent calibration uncertainties. The resulting joint fit is statistically unacceptable and can be rejected with greater than 99 per cent confidence. As expected from Figure 7, examination of the residuals shows that the low count rate state spectra are softer below ≈ 2 keV than the high count rate state spectra. If we add a third blackbody that is unaffected by partial covering to our joint fitting, we can obtain an acceptable joint fit. The third blackbody has a temperature of about 0.5 keV but is poorly constrained.

The fits of the previous paragraph and their residuals could signify either (1) a true change of the blackbody parameters between the low and high count rate states (as well as a partial covering change) or (2) the presence of an additional soft component that is unaffected by the partial covering so that it can be seen during the low count rate state but is diluted away from observability during the high count rate state. As is clear from previous sections, our spectral fits alone cannot formally falsify the first possibility. However, given the observed spatial extent at low energy the additional soft component of the second possibility can naturally be explained as time-delayed X-rays that have been dust scattered into the line of sight by the interstellar medium. For a source at the distance and position of Cir X-1, the time delay is ~ 10 days (see equation 20 of Mauche & Gorenstein 1986), a significant fraction of the orbital period. Replacing the third blackbody of the previous paragraph by a model consisting of the first two blackbodies multiplied by E^{-2} does give a fair fit to the data so indicating that dust scattering is a plausible hypothesis. Our relatively short span of low count rate state data does not allow us to probe sensitively for temporal changes of the soft component due to the decay of the dust halo.

4 DISCUSSION AND SUMMARY

4.1 Partial covering: a direct flux plus electron scattered flux model

Our observations strongly argue that partial covering is a crucial determinant of the behaviour of Cir X-1. We clearly see the spectral features expected from partial covering (Figure 3), and the observed continuum spectral variability is also best explained in terms of it (Figure 5). These two separate effects in conjunction are compelling. As mentioned in Section 3, a large change in the partial covering column without a corresponding change in the partial covering fraction (see Figure 4) is physically somewhat surprising. However, as we describe below, such a change could easily occur if we observed both direct, but attenuated, X-rays as well as

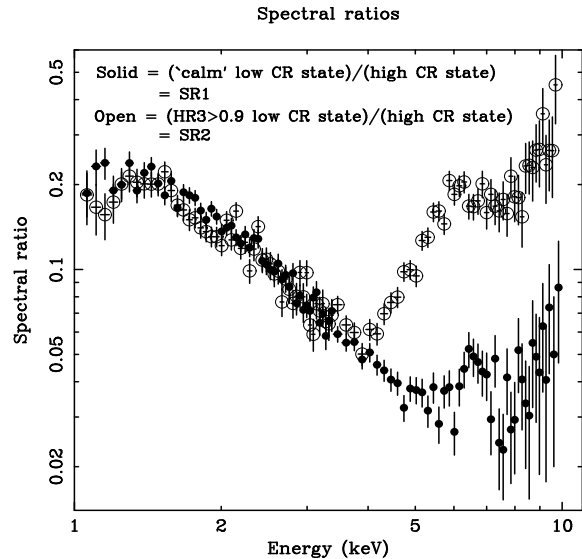


Figure 7. GIS2 spectral ratios as labeled in the diagram (‘CR’ stands for ‘count rate’ and ‘SR’ stands for spectral ratio).

X-rays that are electron scattered around the attenuating matter (this electron scattered component is local to Cir X-1 and totally distinct from the dust scattered component of the previous section). Cir X-1 would then be like a Seyfert 2 galaxy with a Compton-thin and time-variable torus, and the fitted partial covering would really represent total covering plus a significant electron scattered component. Partial covering models have been used to fit Seyfert 2 X-ray spectra (e.g. Iwasawa et al. 1994). As will become clear, the direct flux plus electron scattered flux scenario obviates the geometrically difficult requirement to partially cover an object as small as a neutron star and its inner disc.

In this scenario, the direct X-rays would be completely blocked at low energies but would penetrate through the absorbing matter above ~ 3 –5 keV and thereby imprint the observed iron edge on the spectrum. The absorbing material could be the outer bulge of an accretion disc if the disc is seen *nearly edge-on*, and the column changes could occur as the disc rotates (dynamic changes of the partial coverer are possible as well). For a disc outer radius of ~ 1 solar radius the disc rotation timescale is such that this scenario appears plausible. Several Seyfert 2 galaxies with Compton-thin tori also show large edges from neutral iron (e.g. Awaki et al. 1991).

The electron scattering of X-rays could arise in an accretion disc corona. One potential prediction of models with a large amount of electron scattering is that the disc flux from Cir X-1 may be polarized over the expected interstellar value at wavelengths where the direct emission is highly absorbed (of course, one will also have to take into account polarization dilution by the companion at wavelengths where this is relevant). The polarization fraction should change with time as the absorbing column, and hence the direct contribution, changes. If scattered photons suffered multiple scatterings the polarization could be significantly reduced (indeed, if the Thomson depth of the scattering ‘mirror’ were greatly below unity the implied isotropic luminosity would be prohibitive). If the jets of Cir X-1 are perpendicular to its disc,

one might expect the polarization position angle to be perpendicular to the jet position angle.

From the previous paragraphs and observations of Seyfert 2 galaxies, one might expect to observe very large equivalent width (~ 1 keV) iron K lines from Cir X-1 during the low count rate state. However, it is important to remember that some direct continuum X-rays are able to penetrate through the obscuring matter at the energies of the iron K lines, and these will reduce the line equivalent widths. Furthermore, the solid angle subtended by the accretion disc bulge need not be large, and this would reduce the equivalent width of the iron line from neutral matter. Performing a calculation similar to that shown in figure 1.11 of White, Nagase & Parmar (1995), we find that $\Delta\Omega/2\pi$ must be about 0.1 to explain the iron line equivalent width, which is consistent with what one might expect from the outer bulge of an accretion disc. The ionized iron lines need not be strong if iron atoms in the scattering mirror are *fully stripped* of their electrons, and the large luminosity of Cir X-1 allows iron atom stripping out to radii of $\sim 0.2R_\odot$ or more (we take the Thomson depth to be $\tau \approx 1$ and require the ionization parameter to be $\xi \gtrsim 10^4$ erg cm s $^{-1}$; see Kallman & McCray 1982). Lower atomic number atoms would also be fully stripped and thus would not produce lines.

Finally, one might expect to see a broad iron line and/or smeared edge due to X-ray reflection off the surface of the inner accretion disc (e.g. Ross, Fabian & Brandt 1996 and references therein). No such features are clearly detected (see the bottom panel of Figure 6). There are three possible reasons for the absence of such features: (1) the magnetosphere or an instability disrupts the inner accretion disc so little disc reflection takes place, (2) the disc inclination is high so that the reflection component is relatively weak (see George & Fabian 1991; note this is what we have suggested above) and (3) electron scattering in the corona, if its temperature is $\gtrsim 1$ keV, renders features indistinguishable by Doppler broadening (such Doppler broadening has only a small effect on the continuum shape).

4.2 Partial covering and the abrupt count rate change

Our spectral fitting above suggests a strong reduction in the amount of partial covering during the low to high count rate state transition (see Figure 1 and Figure 6). Furthermore, for our best fits, the partial covering corrected isotropic luminosities (hereafter ‘the true luminosities’) in the low and high count rate states are quite similar (the absorption corrected fluxes are 3.8×10^{-8} erg cm $^{-2}$ s $^{-1}$ and 4.1×10^{-8} erg cm $^{-2}$ s $^{-1}$, respectively). Indeed, we find that for a large region of statistically acceptable chi-squared parameter space the true luminosity of Cir X-1 *need not* change during the observed transition. It is more difficult to prove the stricter statement that the true luminosity of Cir X-1 *does not* change, due to the fact that for very thick partial covering the true luminosity and partial covering percentage are highly covariant quantities (cf. the contours in Figure 4). If the true luminosity of Cir X-1 does not change significantly between the low and high count rate states, Cir X-1 would have been constantly accreting at or perhaps even above the Eddington rate throughout our observation, despite the fact that its count rate varied by about an order of magnitude.

Furthermore, as discussed in section 3.2.3, the underlying spectral shape *need not* change either provided there is a third soft component that is diluted to invisibility once the partial covering is reduced (again it is hard to prove that the underlying spectral shape *does not* change). We note that, despite the lack of strong low energy absorption changes, much of the behaviour studied in Dower, Bradt and Morgan (1982) could also result from partial covering changes provided the partial coverer is so thick that essentially all the X-rays striking it are entirely absorbed. Indeed, the famous figure 4 of Dower et al. (1982) is highly suggestive of partial covering by very thick matter.

However, as discussed by Dower et al. (1982) and other authors, the strong radio and infrared outbursts near zero phase cannot be obviously understood solely in terms of partial covering changes. Furthermore, due to the observed flux rises during the X-ray bursts, we know that the true luminosity of Cir X-1 cannot be the Eddington one at all times. The recent flux rises to 2–3 Crab seen in *RXTE* all-sky monitor data also suggest true luminosity changes. The detailed situation is likely to be very complex, although our observations convincingly demonstrate that some form of partial covering is a key element. It is perhaps possible that the obscuring matter is ejected from the vicinity of the neutron star at the time of zero phase, perhaps to make the radio nebula or jets. Our iron line measurements are consistent with an ejection of matter although the statistics are not good enough to prove that such an ejection must occur (i.e. we cannot show that the line normalization must drop dramatically).

Our observations do not appear to give direct insight into why Cir X-1 accretes at such a remarkable rate, and we have little to add to the theoretical speculation on this issue. It may well be difficult to gain further insight into this matter until the orbital parameters, companion star spectral type, proper motion and neutron star magnetic field of Cir X-1 are better determined. Observations to measure these crucial system parameters are needed.

ACKNOWLEDGMENTS

We gratefully acknowledge financial support from the United States National Science Foundation (WNB) and the Royal Society (ACF). We thank K. Ebisawa, K. Iwasawa, K. Mukai, Ph. Podsiadlowski, R. Ross, R. Shirey, Y. Ueda, N. White, L. Whitlock and R. Wijers for useful discussions. We thank the members of the *ASCA* team who made these observations possible.

REFERENCES

- Awaki H., Koyama K., Inoue H., Halpern J.P., 1991, PASJ, 43, 195
- Brandt W.N., Matt G., 1994, MNRAS, 268, 1051
- Brandt W.N., Podsiadlowski Ph., 1995, MNRAS, 274, 461
- Day C., Jennings D., Seufert E., Watkins R., 1995a, *ASCA* Getting Started Guide for Revision 1 Data: version 4.1, NASA/GSFC
- Day C., Arnaud K., Ebisawa K., Gotthelf E., Ingham J., Mukai K., White N., 1995b, The ABC Guide to *ASCA* Data Reduction: version 4, NASA/GSFC

- Dower R.G., Bradt H.V., Morgan E.H., 1982, *ApJ*, 261, 228
- Ebisawa K., Ueda Y., Inoue H., Tanaka Y., White N.E., et al., 1996, *ApJ*, in press
- Fabian A.C., Rees M.J., Stella L., White N.E., 1989, *MNRAS*, 238, 729
- Frank J., King A., Raine D., 1992, *Accretion Power in Astrophysics*. Cambridge University Press, Cambridge
- George I.M., Fabian A.C., 1991, *MNRAS*, 249, 352
- Gottwald M., Parmar A.N., Reynolds A.P., White N.E., Peacock A., Taylor B.G., 1995, *A&AS*, 109, 9
- Glass I.S., 1994, *MNRAS*, 268, 742
- House L.L., 1969, *ApJS*, 18, 21
- Ikegami T., 1986, PhD thesis, University of Tokyo
- Inoue H., 1989, in White N., Hunt J., Battrick B., eds, *Proc. 23rd ESLAB symp. on two topics in X-ray astronomy*. ESA Publications, Paris, p. 109
- Iwasawa K., Yaqoob T., Awaki H., Ogasaka Y., 1994, *PASJ*, 46, L167
- Kallman T., McCray R., 1982, *ApJS*, 50, 263
- Lampton M., Margon B., Bowyer S., 1976, *ApJ*, 208, 177
- Maisack M., Staubert R., Balucinska-Church M., Skinner G., Döbereiner S., Englhauser J., Sunyaev R., 1995, *Adv. Space Res.*, 16, 91
- Makino Y., 1993, PhD thesis, Osaka University
- Matt G., Fabian A.C., Ross R.R., 1993, *MNRAS*, 262, 179
- Mauche C.W., Gorenstein P., 1986, *ApJ*, 302, 371
- Miyamoto S., Kitamoto S., in Tanaka Y., Lewin W.H.G., eds, *Japan-USA seminar on Galactic and extragalactic compact X-ray sources*. ISAS, Tokyo, p. 187
- Moneti A., 1992, *A&A*, 260, L7
- Morrison R., McCammon D., 1983, *ApJ*, 270, 119
- Oosterbroek T., van der Klis M., Kuulkers E., van Paradijs J., Lewin W.H.G., 1995, *A&A*, 297, 141
- Phinney E.S., 1983, PhD thesis, Cambridge University
- Phinney E.S., Kulkarni S.R., 1994, *ARA&A*, 32, 591
- Predehl P., Schmitt J.H.M.M., 1995, *A&A*, 293, 889
- Press W.H., Flannery B.P., Teukolsky S.A., Vetterling W.T., 1989, *Numerical Recipes in Pascal*. Cambridge University Press, Cambridge
- Ross R.R., 1978, PhD thesis, Univ. of Colorado
- Ross R.R., Fabian A.C., Brandt W.N., 1996, *MNRAS*, 278, 1082
- Shafer R.A., Haberl F., Arnaud K.A., Tennant A.F., 1991, *XSPEC Users Guide*. ESA Publications, Noordwijk
- Shirey R.E., Bradt H.V., Levine A.M., Morgan E.H., 1996, *ApJ*, in press
- Stewart R.T., Nelson G.J., Penninx W., Kitamoto S., Miyamoto S., Nicolson G.D., 1991, *MNRAS*, 253, 212
- Stewart R.T., Caswell J.L., Haynes R.F., Nelson G.J., 1993, *MNRAS*, 261, 593
- Sunyaev R., et al., 1991, *Sov. Astron. Lett.*, 17, 409
- Tanaka Y., Inoue H., Holt S.S., 1994, *PASJ*, 46, L37
- Tashiro M., Fukazawa Y., Idesawa R., Ishisaki Y., Kubo H., Makishima K., Ueda Y., Team G., 1995, *ASCA News*, 3, 9
- Tennant A.F., 1985, *Space Sci. Rev.*, 40, 433
- Tennant A.F., Fabian A.C., Shafer R.A., 1986, *MNRAS*, 221, 27P
- Tennant A.F., 1988a, *Adv. Space Res.*, 8, 397
- Tennant A.F., 1988b, *MNRAS*, 230, 403
- Tsunemi H., Kitamoto S., Manabe M., Miyamoto S., Yamashita K., 1989, *PASJ*, 41, 391
- White N.E., Nagase F., Parmar A.N., 1995, in Lewin W.H.G., van Paradijs J., van den Heuvel E.P.J., eds, *X-ray binaries*. Cambridge Univ. Press, Cambridge, p. 1
- Whitlock L., Tyler P., 1994, *Legacy #4*, The Journal of the High Energy Astrophysics Science Archive Research Center, NASA/GSFC

This paper has been produced using the Royal Astronomical Society/Blackwell Science L^AT_EX style file.